Materials Science in Semiconductor Processing 43 (2016) 123–128

Contents lists available at ScienceDirect

Materials Science in Semiconductor Processing

journal homepage: www.elsevier.com/locate/mssp

Comparative study of Fe doped ZnO based diluted and condensed magnetic semiconductors in wurtzite and zinc-blende structures by first-principles calculations

Bakhtiar Ul Haq [a,b,*], R. Ahmed [a,**], A. Shaari [a], N. Ali [a], Y. Al-Douri [c,d], A.H. Reshak [e,f]

[a] Department of Physics, Faculty of Science, Universiti Teknologi Malaysia, UTM Skudai, 81310 Johor, Malaysia
[b] Department of Physics, Sungkyunkwan University, Suwon 440-746, Korea
[c] Institutes of Nano Electronic Engineering, University Malaysia Perlis, 01000 Kangar, Malaysia
[d] Physics Department, Faculty of Science, University of Sidi-Bel-Abbes, 22000 Algeria
[e] New Technologies-Research Centre, University of West Bohemia, Univerzitni 8, 306 14 Pilsen, Czech Republic
[f] Center of Excellence Geopolymer and Green Technology, School of Material Engineering, Universiti Malaysia Perlis, 01007 Kangar, Malaysia

ARTICLE INFO

Article history:
Received 1 October 2015
Received in revised form
5 December 2015
Accepted 9 December 2015

Keywords:
DFT
Half metallic materials
Magnetic materials
FP-LAPW
Electronic band structure

ABSTRACT

Magnetic semiconductors with simultaneous semiconducting and magnetic characteristics are significant for applications in next generation spintronic devices. However, efficiency of these materials strongly relies on the selection of the proper host and dopant/alloying materials. In this work, we explore magnetic semiconductors based on the most appropriate materials namely ZnO doped with Fe in wurtzite (*w*) and zinc-blende (*zb*) structures. For comprehensive analysis, Fe has been doped into ZnO for several Fe concentrations such as 6.25%, 12.5%, 18.5% and 25%. Investigations are achieved using density functional theory (DFT) based full potential linearized augmented plane wave plus local orbital FP-L (APW+*lo*) method. The exchange correlation energy has been determined using Perdew et al. proposed generalized gradient approximations (GGA) with additional Hubbard (*U*) parameter as well. Our results show that; in *w*-structure, Fe:ZnO favors antiferromagnetism (AFM) at ground state, whereas in *zb* structure, ferromagnetism (FM) is dominated at 6.25% and 12.5% dopant concentration. However, for 18.75% and 25% dopant concentration, AFM interactions are dominated over FM, possibly is caused by the occurrence of anti-ferromagnetic secondary phases. Moreover, effect of mismatching ionic radii of Fe and Zn atoms, and formation of secondary phases is noticed on lattice parameters of Fe:ZnO with Fe concentration. The electronic and magnetic properties of Fe:ZnO endorse them suitable for applications in spin based electronic devices.

1. Introduction

Diluted magnetic semiconductors (DMS) with allied semiconducting and magnetic characteristics have been extensively studied for the past few years. The main motivation behind this is to investigate suitable materials/composition of the magnetic semiconductors with enhanced processing speed and data storage for spintronics [1–3]. DMSs are designed by doping magnetic elements particularly transition metals (TM) in host semiconductor matrix. Therefore, search for appropriate host semiconductor is crucial alongside dopant element. In this regard, ZnO is considered one of the excellent host semiconductor [4], as ZnO exhibit important features like wide and direct band gap, abundant availability and easy fabrication [2,5–9].

ZnO that naturally exist in *w*-structure, now is getting equal importance in meta-stable *zb* geometry for fabrications of DMSs [10–22]. Although considerable research work is available in literature on DMS, there are certain key issues in realizing of DMS for their practical use in devices, like, synthesis of homogeneous DMS, with high T_c. The embedded nano-crystals exhibit different structural geometry than that of host materials. Similarly many TMs display extremely low thermodynamic miscibility in semiconductors and have maximum tendency of impurity dopant aggregation.

By employing advanced characterization tools, it has also been proven that the robust FM in certain DMS can be correlated to the

* Corresponding author at: Department of Physics, Faculty of Science, Universiti Teknologi Malaysia, UTM Skudai, 81310 Johor, Malaysia.
** Corresponding author.
E-mail addresses: bakhtiarjadoon@gmail.com (B. Ul Haq), rashidahmed@utm.my (R. Ahmed).

http://dx.doi.org/10.1016/j.mssp.2015.12.010
1369-8001/

existing nano-scale regions with rich magnetic cations, referred to as condensed magnetic semiconductors (CMS) buried in the matrix of the host [23]. In CMS, the FM clusters can be combined together, resulting in significantly higher total magnetic moment (MM) and stable spin state. This higher MM, from three or four times larger than the MM of a single dopant atom, is due to the alignment of FM clusters [24]. The combined effect of the nanocomposites in magnetic semiconductors, resulting in higher MM, has attracted considerable researcher's attention [23–29].

Among TMs, one of the most important and suitable dopant element to be used in ZnO is the Fe^{2+} for fabrication of ZnO-based DMS for spintronic applications [22,30]. However, there exists certain conflicts between the results that rationalize their practical applications for efficient DMS based on Fe:ZnO. For instance, the experimental studies of Han et al. [31] have reported room temperature FM (RTFM) in Fe:ZnO, which was contradicted soon after by Yoon et al. [32] while predicting that; Fe–Fe interactions are dominated by AFM ordering in Fe:ZnO. Yoon et al. predictions were supported by other researchers as well via first-principles studies at the level of LDA+U [33] and GGA+U [34]. In addition, DFT based hybrid functional calculations performed by Xiao et al. [35] reported antiferromagnetic ordering for Fe^{2+} substituted ZnO materials where the origin of magnetic ordering have been attributed directly to the local ordering of Fe in the ZnO matrix. Similarly in a GGA based first-principles study, McLeod et al. [36] reported that the observed ground state antiferromagnetic ordering was dominated by FM because of secondary phase formation (i.e. $ZnFe_2O_4$). On the other hand, Lin et al. [37] achieved FM in Fe:ZnO above room temperature in an experimental study. In a mixed experimental and theoretical study, Karmakar et al. [38] observed RTFM in Fe:ZnO nanocrystals alongside transformation to spin glass at low temperature, and paramagnetic above 450 K. The corresponding RTFM in Fe:ZnO was reported to be originated from the unequal antiferromagnetic Fe^{3+} ions [39]. Similarly, the experimental investigations of Karamat et al. [40] regarding the magnetic properties of Fe:ZnO have revealed FM nature at 300 K. The investigations of Wang et al. [41], regarding the room temperature ferromagnetic ordering, highlight that the magnetization in Fe:ZnO is strongly dependent on the concentration of the Fe impurities. The concentration of dopant atoms play important role in tuning the properties of magnetic semiconductors as well as in the formation of secondary phases and clusters. Hence increase in concentration of dopant atoms favor to cluster in the matrix of the host semiconductor materials, has become an important question in the study of magnetic semiconductors [42]. To resolve this issue, therfore, the investigations concerning the site preferences in Fe doping ZnO are essential. Moreover, mostly studies reported in literature are focused on the *w*-structure of Fe:ZnO. Fe doped *zb*-structure of ZnO is scarcely explored to our knowledge [22].

In this work, we perform first-principles calculations comprehensively to investigate the structural, electronic and magnetic properties of Fe:ZnO based diluted and condensed magnetic semiconductors in both *w* and *zb* geometry. The well established density functional theory (DFT) based FP-L(APW+*lo*) methodology was used within generalized gradient approximations (GGA) and GGA+Hubbard (*U*) parameter as exchange correlation potentials.

2. Computational method

For the present first-principles calculations of Fe:ZnO, the DFT based FP-L(APW+*lo*) method has been used as implemented in the WIEN2k package [43]. In FP-L(APW+*lo*) method, the unit cell is divided into two regions namely the non-overlapping atomic spheres or core region, and interstitial regions, where different basis sets are used in both the regions to expand the Kohn–Sham wave functions, charge density and potential. Inside the core region, a linear combination of radial functions times spherical harmonics is used, and in the interstitial region a plane wave expansion is used [43]. In this work to treat the exchange correlation energy, Perdew et al. proposed GGA [44] and GGA+*U* [45–47] has been used. The criteria of choosing *U*-parameter has been discussed in detail in the section describing the electronic properties. The muffin-tin radii (RMT) values for Zn^{2+}, Fe^{2+} are selected as 1.78 a.u and 1.5 a.u for O^{2-} atoms. A dense *k*-mesh with 72*k*-points is employed in the special irreducible Brillion zone (BZ). Energy cutoff is taken as $K_{max}=8.0/R_{MT}(R_{yd})^{1/2}$. The Fourier expanded charge density was truncated at $G_{max}=16$ a.u^{-1}.

3. Results and discussion

Results of our calculations are given in Table 1 for the ground state total energies of Fe:ZnO in *w* and *zb* structures. It is noted that the total energies of the investigated structures of Fe:ZnO exhibited marginal difference in both *w* and *zb* structures. These minor differences in *w* and *zb* structures reflecting the equivalent stability of *zb*-Fe:ZnO to that of *w*. Because except the difference in their stacking direction (111) both the structures present similar local tetrahedral bonding and carry the same atomic coordination through the second nearest neighbors as in the case of undoped ZnO [22].

By adopting the approach of Gopal et al. [33], two different spatial arrangements, referred as C1 and C2 based on the Fe substitution sites, are considered for the investigations of the clustering preference, ground state magnetic stability and short range/long range magnetic interactions. In C1 spatial arrangement, the Fe^{2+} dopant atoms are placed at a minimum distance to neighboring Fe^{2+} atoms separated by an oxygen atom i.e. Fe–O–Fe. While in C2 spatial arrangement, the Fe^{2+} atoms are placed far apart from other Fe atoms separated by two oxygen atoms and one Zn atom like Fe–O–Zn–O–Fe. For both arrangements, a marginal difference in the total energies of the two spatial arrangements is noticed. For example, at 12.5% dopant concentration, the total energy values are -3611.9631 and $-3611.9599R_y$ respectively for *w*-Fe:ZnO, and for zb-strucutre, are -3611.9617 and $-3611.9579R_y$ respectively for C1 and C2 arrangements. However comparatively lower energy of the C1 configuration than in the corresponding C2 configuration is noted for all the studied compositions. This trend is analogous for both *w* and *zb* geometries, showing that Fe:ZnO-based DMS favors short-range Fe–Fe magnetic coupling and have a tendency to cluster together. Our results of clustering tendency in *w*-Fe:ZnO are in agreement to Ref. [33].

To investigate the effect of Fe^{2+} on the structural properties of ZnO, lattice parameters are evaluated by minimizing the total energy of the unitcell/Supercell volume through the Murnaghan's equation of state [48]. The results, as presented in Fig. 1, show that there is variation in the lattice parameters for different dopant concentrations. The lattice parameters of Fe:ZnO in *w*-structure do not reveal a significant change for 6.25% and 12.5% of the Fe^{2+} concentration, whereas a drastic decrease in the lattice parameters

Table 1
Summary of the calculated ground-state total energies (in Ry) per formula unit of Fe:ZnO in *w* and *zb* structures.

Composition	*w*	*zb*
$Zn_{15}Fe_1O_{16}$	−3677.3845	−3677.3802
$Zn_{14}Fe_2O_{16}$	−3611.9631	−3611.9617
$Zn_{13}Fe_3O_{16}$	−3546.4452	−3546.3838
$Zn_{12}Fe_4O_{16}$	−3480.9988	−3480.9970

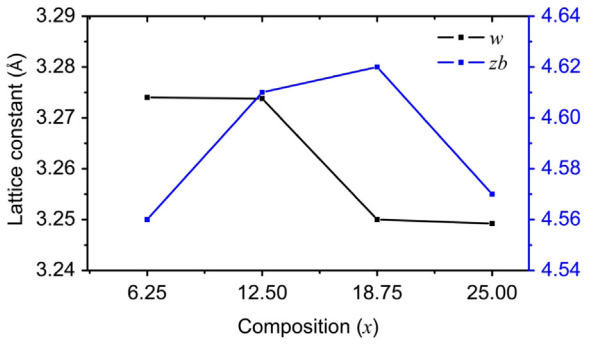

Fig. 1. The variation in the lattice parameter *a* of ZnO in *w* and *zb* structures as a function of Fe^{2+} concentration.

was observed for 18.75% and 25% of Fe^{2+}. Unlike *w*-structure, *zb* structure is comparatively more sensitive to dopant atoms. The lattice parameters of Fe:ZnO experience a significant increment with increasing Fe^{2+} contents, however, by exceeding Fe^{2+} concentration more than 18.75%, the lattice parameters start decreasing. The increment in the lattice parameters of ZnO in the presence of Fe^{2+} atoms is possibly caused by the larger atomic radii of Fe^{2+} (~0.77 Å) than Zn^{2+} (~0.74 Å) that has also been observed experimentally [27,49–50]. Whereas shrinkage found in the lattice parameters of Fe:ZnO (*w* and *zb*) beyond 12.5% and 18.75% respectively reflects the formation of secondary phases in Fe:ZnO. Such reduction in lattice parameters was also reported in other studies as well [27,51].

To investigate the nature of magnetism in the Fe:ZnO, the total energies per formula unit were calculated in both FM and AFM spin modes. To check the FM or AFM ground-state magnetic stability, the difference in the energies of the FM and AFM spin modes is calculated using relation $\Delta E = E_{AFM} - E_{FM}$. According to this relation if $\Delta E > 0$, the material is ferromagnetic in ground state, otherwise AFM is favored. The calculated total energy difference in the FM and AFM states is schematically depicted in Fig. 2. Our calculations for ground state magnetic stability, at the level of GGA+*U*, show AFM ground state of Fe:ZnO in *w*-phases. The existence of AFM interactions in *w*-Fe:ZnO is also reported experimentally [32,52] and other LDA+*U* [33] and GGA+*U* [34,53] calculations. Literature shows that in Fe:ZnO, the nearest neighboring cations favor the antiparallel alignment, and hence the strong AFM interactions can take place [32,54]. Unlike *w*-phase, Fe:ZnO shows dominant ferromagnetic interactions in *zb* phase for 6.25% and 12.5% of Fe^{2+} with GGA+*U* calculations. These ferromagnetic phases respectively exhibit magnetic moments (per formula unit)

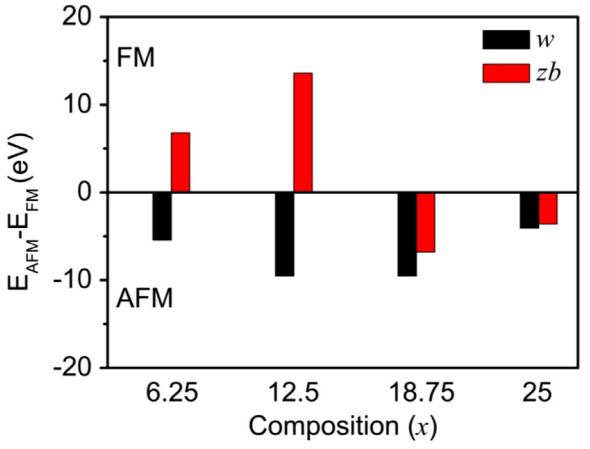

Fig. 2. The schematic representation of the stable FM/AFM ground state of Fe:ZnO with GGA+*U*.

of magnitudes 0.25 μ_B and 0.52 μ_B. The local magnetic moment of Fe^{2+} in the matrix of *zb*-ZnO was calculated as 3.27 μ_B which is in good agreement to the reported value 3.22 μ_B in literature [34]. Since *zb*-ZnO is intrinsically non-magnetic, the occurrence of magnetization by impurity substitution suggests that Fe^{2+} atoms are the main contributor to the observed magnetization. The observed AFM in *zb*-Fe:ZnO for higher Fe^{2+} concentration can be attributed to the appearance of Fe_2O_3 or $ZnFe_2O_4$ secondary phases that are intrinsically antiferromagnetic in ground state [41,55–56]. The unusual variation in the lattice parameters discussed earlier further supports the occurrence of these secondary phases and the resulted AFM mechanism.

DFT calculations based on common exchange correlation potentials are insufficient in describing band structure/band gap particularly related to materials containing the strongly localized electrons such as Zn-*d* states. This problem is even severe in case of transition metals doped ZnO, where the impurity atoms in the host ZnO underestimate the static correlation in the localized orbital and lead to the incorrect metallic description of the electronic structure of ZnO [34]. To investigate the electronic properties of Fe:ZnO in *w* and *zb* structures in terms of their spin polarized DOS, GGA+*U* approach is implemented to treat with exchange correlation potentials because this scheme overcome sufficiently the shortcomings of standard DFT through Hubbard *U*-parameter which is applied to the on-site interaction correction for the Zn-3d and Fe-3d electrons, and reproduces their binding energies nearly equivalent to the experimental results. To select an optimized *U*-value for Zn-3d and Fe-3d electrons, the values of *U*-parameter have been varied between 0 and 10 eV. We observed that by raising the *U*-values, the binding energies increase, and Zn-3d states were shifted downwards that consequently resulted in enhanced energy gap. The dispersion of Zn-3d states with and without *U*-parameter has been shown in Fig. 3. Our analysis reveal that for $U = 7.5$ eV, the Zn-3d electrons are in good agreement with experiment [57] and other theoretical calculations [58]. Similarly, we settled on-site interaction correction $U = 3.5$ eV for Fe-d electrons similar to the recommended value in another studies [34,59], where the exchange parameter is set to the typical value at $J = 1$ eV.

The spin-polarized total DOS and partial DOS of Fe:ZnO system were determined both with GGA and GGA+*U*. Due to resembling DOS profile of Fe:ZnO, optimal spin-polarized total and partial DOS of $Zn_{87.5}Fe_{12.5}O$ are shown here. The metals like electronic

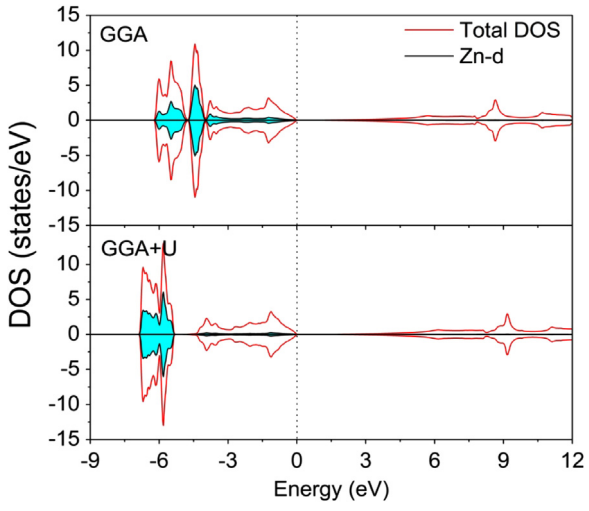

Fig. 3. The spin polarized DOS of ZnO determined with GGA and GGA+*U* descriptions for $U = 7.5$ eV. It can be seen from figure that by applying *U*, the binding energy of Zn *d*-band has been increased near to experimental value.

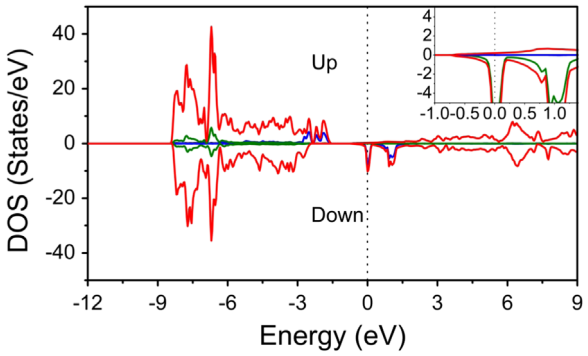

Fig. 4. The spin polarized DOS of Fe:ZnO determined for 12.5% of Fe in *zb* structure determined with GGA. The inset of the figure shows the conduction band minimum where the Fermi level is positioned inside the conduction band reflecting the metal like behavior of Fe:ZnO with GGA.

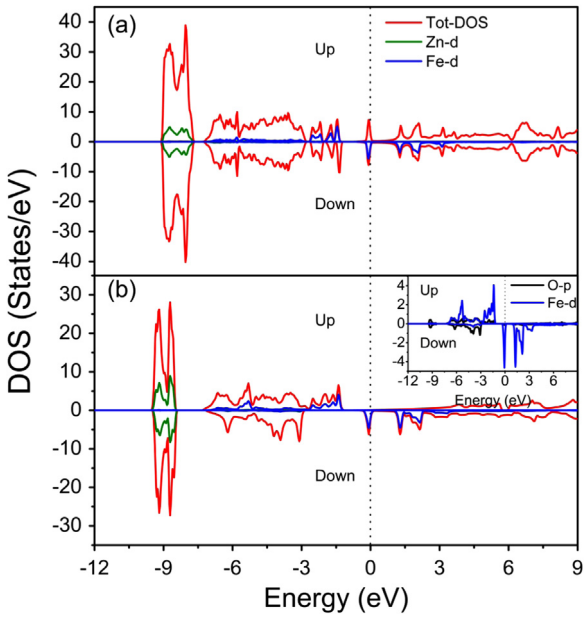

Fig. 5. Spin-polarized total and partial DOS of Fe:ZnO in *w* (a) and *zb* (b) phases at 12.5% Fe contents at the level of GGA+U. (The dotted line reveals the Fermi level; the states in positive energies represent the majority spin carriers and the states in negative energies resemble the minority spin carriers).

behavior of Fe:ZnO can be seen from DOS profile determined with GGA where the Fermi-level appear in CB minimum (Fig. 4). However, this shortcoming of GGA has been rectified at the level of GGA+*U*. Fig. 5 depicts the spin polarized total and partial DOS of Fe:ZnO in *w* and *zb* structures determined with GGA+*U*.

The DOS profile of Fe:ZnO shown in Figs. 4 and 5, was found significantly different than that of ZnO shown in Fig. 3. Impurity bands have been observed in the vicinity of Fermi level of Fe:ZnO. As can be seen from (Fig. 5(b)), in *w*-structure where the Fe:ZnO favor AFM in ground state, the consecutive Fe^{2+} atoms are arranged such that their spin directions are fixed anti-parallel to each other. In case of *zb* structure (Fig. 5(b)), the arrangement of impurity bands in the vicinity of Fermi level is however different than *w*-structure. By introducing the *U* parameter to Zn^{2+} and Fe^{2+} *d*-electrons, gap is found in between VBM and CBM for majority spins states. A significant impurity band appears over Fermi level for minority spin states that shows a complete spin polarization of the majority and minority spin carriers in the vicinity of Fermi level. This feature of $Zn_{87.5}Fe_{12.5}O$ characterizes it as half metallic material in *zb* phase. In both the spin-up and spin-down configurations, the Zn-*d* states appear at deep VB at energy

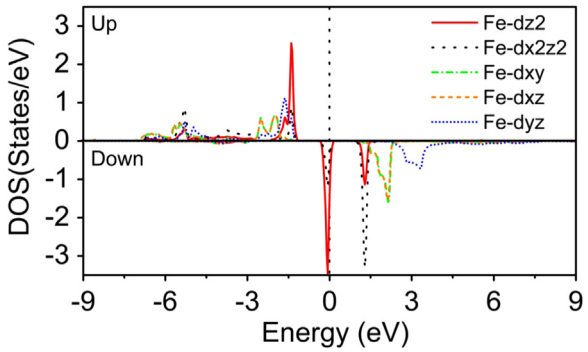

Fig. 6. Splitting of Fe d-band into e_g and t_{2g} states due to the Coulomb potential produced by O^{2-} atoms.

limits from ~−9.0 to ~−7.72 eV (~−9.47 to −8.44 eV in *zb*) relative to Fermi level. Hence, the contribution of the Zn-*d* states to the electronic properties of Fe:ZnO in both structural geometries is almost negligible in ground state. The majority spins Fe-3d states exhibit different dispersion for AFM mode in *w* and FM mode in *zb* structure. A relatively large dispersion of Fe^{2+} *d*-band has been observed in FM (~−7.1 to −1 eV) mode compared to AFM (~−2.68 to −1.25). The narrower width of the occupied Fe^{2+} *d*-band is due to the fact that it can't mix to its neighboring Fe^{2+} atoms that carry anti-parallel spin alignment. Similar results for impurity *d*-band dispersion in FM and AFM is also reported by Sato et al. [60] in Mn:ZnO. For minority spin; Fe-3d states are partially localized in the Fermi level and in CB at ~0.9 to 3 eV (~1 to 3.6 eV in *zb* phase).

Moreover, the O^{2-} ions that surround the Fe^{2+} ions in a tetrahedron in the host matrix induce a negative coulomb potential around Fe^{2+} ions. As a result, the crystal field effect is generated that has lead the splitting of Fe^{2+} *d*-band into sub-bands in terms of doublet e_g (dx^2–dy^2 and dz^2) and triplet t_{2g} (dxy, dzx, dyz) orbital. A schematic overview of Fe^{2+} *d*-band splitting is shown in Fig. 6. The energies of the e_g and t_{2g} bands strongly depend on the geometry of the crystal. In *w* and *zb* geometry, the O^{2-}-ions provide a tetrahedral Coulomb environment, where t_{2g} states reside closer to O^{2-} and thus are higher in energy compared to e_g states. For majority spins, both e_g and t_{2g} states are localized in the VB, where for minority spins, the e_g states are partially localized in the Fermi level at 2 eV relative to Fermi-level in the CB. On the other hand, t_{2g} states are positioned in the CB for minority spin states. Our results for DOS profile in *zb*-structure are well matching to that of Mamouni et al. [22].

It is important to note that the DOS profile of Fe^{2+} *d*-band and O^{2-} *p*-band do not experience any significant hybridization as shown in the inset of Fig. 5(b). This suggest that the FM interactions in Fe:ZnO for 6.25% and 12.5% in *zb* structures are not mediated by O-p electrons and hence the FM in these DMS cannot be defined by the double exchange mechanism as reported in Fe:ZnO nanowire as well [34]. A literature review shows that the FM observed in magnetic semiconductors, particularly in doped ZnO, is real and is believed to be caused by free charge carriers that mediate exchange interactions between the local magnetic dopant sites originated from magnetic impurity atoms. This mediation of magnetism is considered to be dependent on the concentration of magnetic impurity [61–64]. To understand the origin of FM/AFM further, some other models have also been employed. According to phenomenological Zener/Ruderman–Kittel–Kasuya–Yosida (RKKY) [65] model, interactions are favoring FM because Fe:ZnO is found to be more stable in C1 similar to some other DMS studies [34,41,66]. Whereas AFM in the Fe:ZnO-based DMS is endorsed due to superexchange interactions and the formation antiferromagnetic secondary phases.

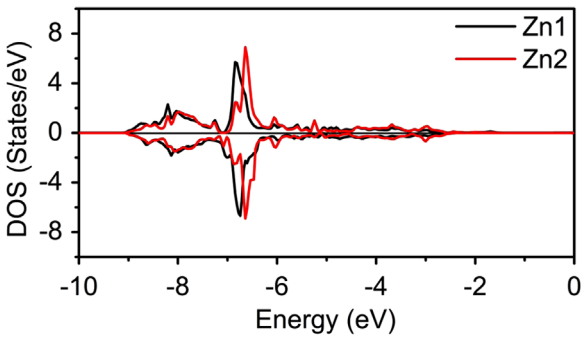

Fig. 7. The schematic overview of Zn d-band. Zn1 atom is coordinated to Fe atoms by one O^{2-} and Zn2 atom is connected to Fe two O^{2-} and on Zn^{2+} ions.

We further investigated the effect of Fe^{2+} impurity atoms on the *d*-electrons of Zn^{2+} located near to and far apart from the substituted Fe^{2+} site. The Zn^{2+} atoms located at near to Fe^{2+} were labeled as Zn1 where they were coordinated to Fe^{2+} by an O-anion such as Zn–O–Fe–O–Zn. The Zn^{2+} atoms located at the larger distance from Fe^{2+} were labeled Zn2 and were coordinated to Fe^{2+} by two O^{2-} atoms and one Zn^{2+} atom. The DOS of Zn1 and the DOS of the Zn2 are shown in Fig. 7. The Zn2 *d*-electrons distant from the Fe^{2+} atoms were found to carry lower binding energy and are positioned mainly at ~ -6.65 eV, however Zn1 *d*-electrons that carry comparatively higher binding energies are positioned at ~ -6.83 eV. The higher binding energy of the Zn1 *d*-electrons than that of Zn2 is possibly due to their smaller distance from the Fe^{2+} atoms, where they experience comparatively higher Coulomb repulsion from the iso-electronic Fe^{2+} atoms that pushed them in the deep VB.

4. Conclusions

In summary, *w* and *zb* structured Fe:ZnO based diluted and condensed magnetic semiconductors have been comprehensively explored using DFT based FP-L(APW+*lo*) method. The magnetic semiconductors based on w-structured Fe:ZnO exhibited antiferromagnetic character in ground state, whereas they favor ferromagnetic interactions in zb structure for lower Fe doping concentration. However, the CMS based on ZnO are antiferromagnetic for both *w* and *zb* structure possibly due to the appearance of antiferromagnetic secondary phases such as Fe_2O_3 and $ZnFe_3O_4$. The ferromagnetic DMS in *zb* structure showed semiconducting nature for majority spin carries and metallic nature for minority spin carriers. The distinguished response for majority and minority spin carriers of the simple *zb* structures (free from several unwanted built-in field and quantum mechanical effects) reflect their importance for applications in spin based electronic device such as spin valves, filters, spin transistors and spin LEDs etcetera.

Acknowledgment

Authors (Bakhtiar Ul Haq, R. Ahmed and A. shaari) would like to acknowledge for the financial support of the Ministry of Education (MOE)/Universiti Teknologi Malaysia (UTM) through Grant nos. Q.J130000.2526.02H89; R.J130000.7826.4F113 and Q.J130000.2526.04H14. Y.A. would like to acknowlegde University Malaysia Perlis for Grant no. 9007-00111 and TWAS-Italy for the full support of his visit to JUST-Jordan under TWAS-UNESCO Associateship. For the author A. H. Reshak, the result was developed within the CENTEM project, Reg. no. CZ.1.05/2.1.00/03.0088, co-funded by the ERDF as part of the Ministry of Education, Youth and Sports OP RDI program. Computational resources were provided by MetaCentrum (LM2010005) and CERIT-SC (CZ.1.05/3.2.00/08.0144) infrastructures.

References

[1] J. Coey, et al., Anisotropy of the magnetization of a dilute magnetic oxide, J. Magn. Magn. Mater. 290 (2005) 1405–1407.
[2] Ü. Özgür, et al., A comprehensive review of ZnO materials and devices, J. Appl. Phys. 98 (4) (2005) 041301.
[3] R. Torquato, et al., Synthesis and structural, magnetic characterization of nanocrystalline $Zn_{(1-x)}Mn_{(x)}O$ diluted magnetic semiconductors (DMSs) synthesized by combustion reaction, Ceram. Int. 40 (5) (2014) 6553–6559.
[4] T. Dietl, et al., Zener model description of ferromagnetism in zinc-blende magnetic semiconductors, Science 287 (5455) (2000) 1019–1022.
[5] U. Ozgur, D. Hofstetter, H. Morkoc, ZnO devices and applications: a review of current status and future prospects, Proc. IEEE 98 (7) (2010) 1255–1268.
[6] Y. Al-Douri, et al., Structural and optical investigations of In doped ZnO binary compound, Mater. Express 4 (2) (2014) 159–164.
[7] N. Hassan, M. Hashim, Y. Al-Douri, Morphology and optical investigations of ZnO pyramids and nanoflakes for optoelectronic applications, Optik -Int. J. Light. Electron Opt. 125 (11) (2014) 2560–2564.
[8] M. Kashif, et al., Characterisation, analysis and optical properties of nanostructure ZnO using the sol-gel method, Micro Nano Lett. IET 7 (2) (2012) 163–167.
[9] N. Hassan, et al., Current dependence growth of ZnO nanostructures by electrochemical deposition technique, Int. J. Electrochem. Sci. 7 (2012) 4625–4635.
[10] J. Zhang, et al., First principles calculations of Co-doped zinc-blende ZnO magnetic semiconductor, Phys. B: Condens. Matter 405 (6) (2010) 1447–1451.
[11] A. Ashrafi, C. Jagadish, Review of zincblende ZnO: stability of metastable ZnO phases, J. Appl. Phys. 102 (7) (2007) 071101.
[12] A. Ashrafi, et al., Growth and characterization of hypothetical zinc-blende ZnO films on GaAs (001) substrates with ZnS buffer layers, Appl. Phys. Lett. 76 (5) (2000) 550–552.
[13] A. Ashrafi, et al., Role of ZnS buffer layers in growth of zincblende ZnO on GaAs substrates by metalorganic molecular-beam epitaxy, J. Cryst. growth 221 (1) (2000) 435–439.
[14] M.V. Limaye, et al., Epitaxially grown zinc-blende structured Mn doped ZnO nanoshell on ZnS nanoparticles, Mater. Res. Bull. 44 (2) (2009) 339–344.
[15] N. Mamouni, et al., Electronic and magnetic structures of V-doped zinc blende Zn1 − xVxNyO1 − y and Zn1 − *x*V*x*P*y*O1 − *y*, Chin. Phys. B 20 (8) (2011) 087504.
[16] D. Xu, et al., Half-metallic ferromagnetism in C-doped zinc-blende ZnO: a first-principles study, Chin. Phys. B 22 (4) (2013) 047507.
[17] X. Li, et al., Half-metallic ferromagnetism in Cu-doped zinc-blende ZnO from first principles study, J. Magn. Magn. Mater. 324 (4) (2012) 584–587.
[18] B.U. Haq, et al., Structural, electronic, and magnetic properties of Co-doped ZnO, Chin. Phys. B 21 (9) (2012) 097101.
[19] B.U. Haq, R. Ahmed, S. Goumri-Said, Tailoring ferromagnetism in chromium-doped zinc oxide, Mater. Res. Express 1 (1) (2014) 016108.
[20] B. Ul Haq, et al., First-principles investigations of Mn doped zinc-blende ZnO based magnetic semiconductors: materials for spintronic applications, Mater. Sci. Semicond. Process 29 (2014) 256–261.
[21] B. Ul Haq, et al., GGA+U investigations of impurity d-electrons effects on the electronic and magnetic properties of ZnO, J. Magn. Magn. Mater. 362 (2014) 104–109.
[22] N. Mamouni, et al., A comparative first-principles study of Fe-, Co-and FeCo-doped ZnO with wurtzite and zinc blende structures, J. Supercond. Novel Magn. 25 (5) (2012) 1579–1587.
[23] A. Bonanni, T. Dietl, A story of high-temperature ferromagnetism in semiconductors, Chem. Soc. Rev. 39 (2) (2010) 528–539.
[24] F. Filippone, et al., Clusters and magnetic anchoring points in (Ga, Fe) N condensed magnetic semiconductors, Phys. Rev. Lett. 107 (19) (2011) 196401.
[25] S. Von Molnár, Spin electronics: from concentrated to diluted magnetic semiconductors and beyond, J. Supercond. 16 (1) (2003) 1–5.
[26] S.-s Yan, et al., Ferromagnetism and magnetoresistance of Co–ZnO inhomogeneous magnetic semiconductors, Appl. Phys. Lett. 84 (13) (2004) 2376–2378.
[27] I. Bilecka, et al., Microwave-assisted nonaqueous sol − gel chemistry for highly concentrated ZnO-based magnetic semiconductor nanocrystals, J. Phys. Chem. C 115 (5) (2011) 1484–1495.
[28] L.-J. Chen, et al., Effect of biaxial strain on half-metallicity of transition metal alloyed zinc-blende ZnO and GaAs: a first-principles study, J. Phys. D.: Appl. Phys. 44 (20) (2011) 205002.
[29] T. Xu, et al., Above-gap and subgap differential conductance anomaly in concentrated magnetic semiconductor Zn 0.32 Co 0.68 O 1 − v/Pb superconductor hybrid junctions, Phys. Lett. A 378 (5) (2014) 602–607.
[30] H. Cao, et al., First-principles study on electronic and magnetic properties of (Mn, Fe)-codoped ZnO, J. Magn. Magn. Mater. 352 (2014) 66–71.
[31] S. Han, et al., A key to room-temperature ferromagnetism in Fe-doped ZnO: Cu, Appl. Phys. Lett. 81 (22) (2002) 4212–4214.
[32] S. Yoon, et al., Magnetic properties of ZnO-based diluted magnetic semiconductors, J. Appl. Phys. 93 (10) (2003) 7879–7881.

[33] P. Gopal, N.A. Spaldin, Magnetic interactions in transition-metal-doped ZnO: An ab initio study, Phys. Rev. B 74 (9) (2006) 094418.
[34] S. Ghosh, et al., Magnetism in ZnO nanowire with Fe/Co codoping: First-principles density functional calculations, Phys. Rev. B 81 (23) (2010) 235215.
[35] J. Xiao, et al., Temperature-mediated magnetism in Fe-doped ZnO semiconductors, J. Phys. Chem. C 117 (10) (2013) 5338–5342.
[36] J. McLeod, et al., Local structure of Fe impurity atoms in ZnO: bulk versus surface, J. Phys. Chem. C 118 (10) (2014) 5336–5345.
[37] Y. Lin, et al., Fe-doped ZnO magnetic semiconductor by mechanical alloying, J. Alloy. Compd. 436 (1) (2007) 30–33.
[38] D. Karmakar, et al., Ferromagnetism in Fe-doped ZnO nanocrystals: experiment and theory, Phys. Rev. B 75 (14) (2007) 144404.
[39] T. Kataoka, et al., Electronic structure and magnetism of the diluted magnetic semiconductor Fe-doped ZnO nanoparticles, J. Appl. Phys. 107 (3) (2010) 033718.
[40] S. Karamat, et al., Structural, optical and magnetic properties of $(ZnO)_{1-x}(MnO_2)_x$ thin films deposited at room temperature, Appl. Surf. Sci. 254 (22) (2008) 7285–7289.
[41] Y. Wang, et al., Ferromagnetism in Fe-doped ZnO bulk samples, J. Magn. Magn. Mater. 320 (8) (2008) 1423–1426.
[42] Q. Wang, et al., Magnetism and energetics of Mn-Doped ZnO (10 $\bar{1}$ 0) thin films, Phys. Rev. B 69 (23) (2004) 233310.
[43] P. Blaha, et al., WIEN2k. An Augmented Plane Wave Plus Local Orbitals Program for Calculating Crystal Properties, Vienna University of Technology, Austria, 2001.
[44] J.P. Perdew, K. Burke, M. Ernzerhof, Generalized gradient approximation made simple, Phys. Rev. Lett. 77 (18) (1996) 3865.
[45] A. Liechtenstein, V. Anisimov, J. Zaanen, Density-functional theory and strong interactions: orbital ordering in Mott-Hubbard insulators, Phys. Rev. B 52 (8) (1995) R5467.
[46] V.I. Anisimov, J. Zaanen, O.K. Andersen, Band theory and Mott insulators: Hubbard U instead of Stoner I, Phys. Rev. B 44 (3) (1991) 943.
[47] V.I. Anisimov, F. Aryasetiawan, A. Lichtenstein, First-principles calculations of the electronic structure and spectra of strongly correlated systems: the LDA+U method, J. Phys.: Condens. Matter 9 (4) (1997) 767.
[48] F. Murnaghan, The compressibility of media under extreme pressures, Proc. Natl. Acad. Sci. U.S.A. 30 (9) (1944) 244.
[49] H. Gu, Y. Jiang, M. Yan, Defect-induced room temperature ferromagnetism in Fe and Na co-doped ZnO nanoparticles, J. Alloy. Compd. 521 (2012) 90–94.
[50] S. Kolesnik, B. Dabrowski, J. Mais, Structural and magnetic properties of transition metal substituted ZnO. arXiv preprint cond-mat/0312233, 2003.
[51] J. Beltrán, et al., Magnetic properties of Fe doped, Co doped, and Fe+Co co-doped ZnO, J. Appl. Phys. 113 (17) (2013) 17C308.
[52] L.Md.C. Pereira, et al., Paramagnetism and antiferromagnetic interactions in single-phase Fe-implanted ZnO, J. Phys.: Condens. Matter 25 (41) (2013) 416001.
[53] N. Ganguli, I. Dasgupta, B. Sanyal, Electronic structure and magnetism of transition metal doped Zn12O12 clusters: role of defects, J. Appl. Phys. 108 (12) (2010) 123911.
[54] L. Pereira, et al., Searching for room temperature ferromagnetism in transition metal implanted ZnO and GaN, J. Appl. Phys. 113 (2) (2013) 023903–023903-9.
[55] J.H. Shim, et al., Origin of ferromagnetism in Fe-and Cu-codoped ZnO, Appl. Phys. Lett. 86 (8) (2005) 82503.
[56] S. Karamat, et al., Structural, elemental, optical and magnetic study of Fe doped ZnO and impurity phase formation, Prog. Nat. Sci.: Mater. Int. 24 (2) (2014) 142–149.
[57] D. Vogel, P. Krüger, J. Pollmann, Self-interaction and relaxation-corrected pseudopotentials for II-VI semiconductors, Phys. Rev. B 54 (8) (1996) 5495.
[58] P. Erhart, K. Albe, A. Klein, First-principles study of intrinsic point defects in ZnO: role of band structure, volume relaxation, and finite-size effects, Phys. Rev. B 73 (20) (2006) 205203.
[59] S. Lany, H. Raebiger, A. Zunger, Magnetic interactions of Cr−Cr and Co−Co impurity pairs in ZnO within a band-gap corrected density functional approach, Phys. Rev. B 77 (24) (2008) 241201.
[60] K. Sato, H. Katayama-Yoshida, Material design for transparent ferromagnets with ZnO-based magnetic semiconductors, Jpn. J. Appl. Phys. 39 (6B) (2000) L555.
[61] J. Lu, et al., p-Type conduction in N–Al co-doped ZnO thin films, Appl. Phys. Lett. 85 (15) (2004) 3134–3135.
[62] W. Liu, X. Tang, Z. Tang, Effect of oxygen defects on ferromagnetism of Mn doped ZnO, J. Appl. Phys. **114** (12) (2013) 123911–123911-6.
[63] W. Liu, et al., Oxygen defects mediated magnetism of Ni doped ZnO, Adv. Condens. Matter Phys. 2013 (2013) , p. 424398.
[64] X. Wang, et al., Effect of the magnetic order on the room-temperature band-gap of Mn-doped ZnO thin films, Appl. Phys. Lett. 102 (10) (2013) 102112–102112-4.
[65] M.A. Ruderman, C. Kittel, Indirect exchange coupling of nuclear magnetic moments by conduction electrons, Phys. Rev. 96 (1) (1954) 99.
[66] M.S. Park, B. Min, Ferromagnetism in ZnO codoped with transition metals: Zn 1−x (FeCo) x O and Zn 1−x (FeCu) x O, Phys. Rev. B 68 (22) (2003) 224436.